International Journal of Innovative Research and Scientific Studies, 8(12) 2025, pages: 95-107

ISSN: 2617-6548

URL: www.ijirss.com

Calculation of the Luneberg optical lens and applications

Arkady Khorunzhenko[1], Mikhail Lavrentiev[2*], Andrey Marchuk[3]

[1,2]*Institute of Automation and Electrometry SB RAS, Novosibirsk, Russian Federation; Novosibirsk State University, Novosibirsk, Russian Federation.*
[3]*Institute of Computational Mathematics and Mathematical Geophysics SB RAS, Novosibirsk, Russian Federation; Novosibirsk State University, Novosibirsk, Russian Federation.*

Corresponding author: Mikhail Lavrentiev (*Email: mmlavrentiev@gmail.com*)

Abstract

This paper presents a numerical approach for designing radially symmetric Luneburg lenses with arbitrary source and image positions. The method reconstructs the refractive index distribution by inverting an Abel-type relation and uses adaptive Gauss–Kronrod quadrature to ensure high accuracy without manual tuning. The algorithm is validated against the classical Luneburg profile and applied to two focusing scenarios: transformation of a plane wave into a converging wave with a prescribed focal distance, and focusing of radiation from a finite-distance point source to a target point. Ray tracing with an explicit Euler scheme and Huygens-based wavefront simulations confirm that an initially planar front segment collapses precisely to the designed focus. Using the optical–hydrodynamic analogy, the obtained refractive index distribution is converted into a seamount depth profile, and nonlinear shallow-water simulations demonstrate significant wave amplitude amplification near the predicted focal area. The results provide a universal framework for the synthesis of gradient-index lenses and offer practical insights into tsunami wave focusing caused by natural seabed topography.

Keywords: Abel transform inversion, Bathymetry, Geometrical optics, Huygens principle, Luneburg lens, MacCormack scheme, Ray tracing, Refractive index profiling, Shallow-water equations, Tsunami focusing.

DOI: 10.53894/ijirss.v8i12.11018
Funding: The study was supported by the project FSUS-2025-0011.
History: Received: 15 October 2025 / **Revised:** 14 November 2025 / **Accepted:** 18 November 2025 / **Published:** 5 December 2025

Competing Interests: The authors declare that they have no competing interests.
Authors' Contributions: All authors contributed equally to the conception and design of the study. All authors have read and agreed to the published version of the manuscript.
Transparency: The authors confirm that the manuscript is an honest, accurate, and transparent account of the study; that no vital features of the study have been omitted; and that any discrepancies from the study as planned have been explained. This study followed all ethical practices during writing.
Publisher: Innovative Research Publishing

1. Introduction

Wave focusing can be defined as the simultaneous arrival of various segments of the wavefront at any point in the region or in its vicinity. Focusing of optical and other waves in media with inhomogeneous conductivity (the speed of propagation of waves in media) can occur due to refraction at the interfaces in media with piecewise constant conductivity

or due to refraction in media where the change in the speed of waves propagation occurs continuously [1]. The first type includes optical lenses made of a homogeneous material with a conductivity different from the environment. An example is glass or plastic lenses used in optical devices. The second type is more difficult to manufacture, when a continuous change in conductivity is approximately realized by the layered structure of the lens [2, 3]. An example of this type is a spherical (in the two-dimensional case, cylindrical) Luneberg lens, in which the conductivity of the medium continuously decreases from the boundaries of the lens to its center, where it reaches its minimum [4]. This lens focuses a radial wave that is outgoing from a point located at a distance R_1 from the center of the lens to a point located at a distance R_2 from the center of the lens on the other side. If R_1 is equal to infinity, then this lens focuses the plane wave to a single point.

In addition to optics, the results of this study can be applied in tsunami forecasting, where a seamount serves as a lens in optics and can focus wave energy at some point behind this bottom irregularity.

2. Materials and Methods

2.1. Calculation of a Round Lens Focusing a Plane Wave to a Single Point

To describe the kinematics of wavefronts in a two-dimensional inhomogeneous medium, where the propagation velocity *c(x,y)* of the wave (conductivity) varies depending on the location, the well known Eikonal Equation 1 is used:

$$f_x^2 + f_y^2 = \frac{1}{c^2(x,y)} = n^2(x,y). \quad (1)$$

Here *c(x,y)* is the wave propagation velocity at point *(x,y)*, and the function *f(x,y)* describes the wavefront line. The value of *n*, which is inverse to the conductivity of the medium, is sometimes called the refractive index of the medium. Equation 1 is the key equation of geometric optics. It allows us to describe the wave front as a family of curves *t = f(x,y)*, where *t* stands for time. The wave rays are orthogonal to the wave-front lines at each moment in time.

Suppose that in a homogeneous space with optical conductivity $c = c_0$ there is an area in the form of a circle with radius R_0, where the conductivity of the medium *c(r)* increases monotonously with the distance *r* to the center up to the value c_0. Here, the conductivity of the medium is understood as the propagation velocity of perturbations. For optics, it is the speed of light in a given medium. The task is to find a radially dependent distribution of optical conductivity inside this circular lens, which implements the focusing of a plane wave to a single point located at a given distance R_1 from the center of the lens. Luneberg studied such a lens for the first time, but the solution he found is written out in parametric form and is not directly suitable for determining the lens parameters [4]. The article describes a numerical algorithm for determining the lens parameters (the distribution of conductivity inside the lens) for specified focal lengths and lens sizes R_0. To simplify the solution, it is assumed that the conductivity of the medium is *c(x,y)* (as well as the refractive index *n(x,y)=1/c(x,y)*) outside the lens, is equal to *1*, and the radius of the lens R_0 is also equal to *1*. If the lens has a radius equal to *b*, then in all formulas, instead of the distance to the center of the lens, *R*, the value *R/b* must be set.

Let us consider the problem in the two-dimensional case. It is required to build a round (in the three-dimensional case, it will be a spherical) Luneberg lens that focuses rays from a point source located to the left of the lens at a distance R_1 from its center to the focus point, which is located to the right of the lens at a distance R_2 from its center (see the diagram in Figure 1, taken from [4]).

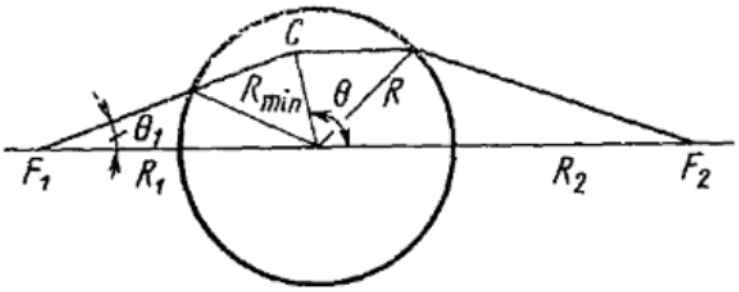

Figure 1.
Diagram of the ray path from point F_1 to point F_2 in the Luneberg lens.
Source: Zelkin and Petrova [4]

The solution to this problem was obtained by Luneberg in a rather complex parametric form. An explicit dependence of *n* on *R* is easily obtained only for an ordinary Luneberg lens, when one source is located on the surface of the lens, that is, $R_1 = 1$, and the other at infinity ($R_2 = \infty$). In this case, the lens transforms a spherically diverging wave into a flat one. Conversely, a plane wave is focused to a single point on the back surface of a spherical lens. For this case, a simple formula is given for the dependence of the refractive index of the medium *n* (the inverse velocity of disturbance propagation) on the distance R to the center of the lens:

$$n = \sqrt{2 - R^2},\ 0 \le R \le R_0. \quad (2)$$

As follows from this formula, the refractive index *n* varies from $2^{1/2}$ in the center of the lens, where *R = 0*, to *1* at its

boundary and in the rest of the area. For the more general case, when $R_1 = \infty$ and R_2 exceeds the radius of the lens, the following formulas are given in Zelkin and Petrova [4] to calculate the dependence of the refractive index *n* on the distance *R* to the center of the lens

$$n = e^{q(\rho,R_2)}. \quad (3)$$

Here, the distance to the center of the lens *R* is related to ρ by the ratio $\rho = nR$. It follows that $R = \rho \cdot e^{(-q\rho,R2))}$, and the value of q is calculated as an integral

$$q(\rho, a) = \frac{1}{\pi}\int_{\rho}^{1} \frac{arcsin(t/a)}{\sqrt{t^2-\rho^2}}\, dt. \quad (4)$$

2.2. Constructing of the Luneberg Lens

2.2.1. Integral Statement of the Luneberg Problem for Arbitrary Radii of the Source and Image

The classical Luneberg lens is a spherical structure of radius *a* with a smooth radial change in the refractive index. The profile of such a lens is given by the analytical formula (2). Such a distribution ensures the transformation of a plane wave incident on the lens into a spherical one converging to a focus at the opposite point of the surface.

More generally, when it is required to associate a source sphere of radius R_{src} and an image sphere of radius R_{img}. There is no analytical formula. The problem is reduced to solving the inverse problem of geometric optics: it is necessary to find the profile $n(R)$ at which the total angle of deflection of rays with different parameters ρ coincides with the specified one. In a spherically symmetric medium, the "optical moment" is preserved $\rho = n(R)R \cdot \sin\theta$, and it is through that that all trajectories are expressed.

This formulation leads to the Abel integral transformation Abel [5] which relates the angular function *Φ(ρ)* to the distribution of the refractive index. Inverting the Abel integral gives the following expression

$$q(\rho, a) = \frac{1}{\pi}\int_{\rho}^{a} \frac{\Phi_{src}(t;R_{src})+\Phi_{img}(t;R_{img})}{\sqrt{t^2-\rho^2}}\, dt, \quad (5)$$

where Φ_{src} and Φ_{img} describe the geometry of the source and image, respectively.

In the classical case (plane wave is focused on the lens' back surface), the contribution of the source goes to zero, and the integrand function is reduced to one arcsin, which gives the known analytical formula (4). More generally, when conditions for the sphere and source radiuses R_{src} and R_{img} are simultaneously taken into account, these two contributions are summed up. That is why the sum of the phases appears in the integral $\Phi_{src}(t; R_{src})+\Phi_{img}(t; R_{img})$: it reflects the need to satisfy both boundary conditions simultaneously. Φ is given by the following formula

$$\Phi = \begin{cases} arcsin(t/R), t < R \\ \pi/2, t \geq R \end{cases}$$

The refractive index profile then is reconstructed from the function $q(\rho, a)$*:* $n(\rho) = exp\,(q(\rho, a))$ (6)

$$R = \rho/n(\rho). \quad (7)$$

By sorting the pairs *(R,n)*, the desired radial profile $n(R)$ is constructed, and the wave propagation velocity is set as

$$c(R) = 1/n(R). \quad (8)$$

2.2.2. Numerical Realization

The analytical expression of the profile exists only for the classical Luneberg lens. In general, the problem is reduced to the numerical calculation of the Abel integral (5), which describes the relationship between the radial coordinate and the refractive index. Since there is no analytical solution for the general case, the profile n(R) is determined by numerical integration.

The interval of the auxiliary radius $\rho \in [0, a]$ is sampled by a uniform rectangular grid containing from *200* to *800* rows and columns. This resolution ensures stable convergence of the results and allows accurate reproduction of the profile shape during subsequent interpolation. For each value of ρ, the integral (5) is calculated, which has a weak singularity as $t \to \rho$. To eliminate this feature and improve accuracy, the Gauss–Kronrod method [6] was used, which has a built-in adaptation of the number of nodes and automatic error estimation. This approach avoids manual selection of the number of integration points and ensures the required accuracy even with an unevenly varying integral expression.

The Kronrod method is especially effective when, after replacing a variable (performed to eliminate a singularity at $t = \rho$) the integrand remains smooth, but it changes unevenly. In addition, the chosen scheme is well combined with adaptive integrators implemented in modern numerical libraries, for example, in the **quad** function [6] of the SciPy package in Python language. This ensures stability during repeated calculations of the integral and makes it easy to include the procedure in the numerical contour of the lens profile.

After calculating the function $q(\rho,a)$ the refractive index is determined by formula (6), and the physical radius is determined by expression (7). The resulting pairs (R, n) are sorted by increasing radius, duplicate values are excluded, and a monotonic profile $n(R)$ is formed. Next, this profile is interpolated and used to construct a two-dimensional velocity field according to expression (8). Outside the lens area, a constant value of the refractive index corresponding to a homogeneous medium is set.

For the control scenario, "plane wave — focus at a distance R_f " ($R_{src} \to \infty$, $R_{img} = R_f$) The numerically obtained profile coincides with the analytical law (2), and the relative discrepancy does not exceed 10^{-6}, which confirms the correctness of the proposed algorithm.

Earlier in the literature [7] the Gauss–Legendre method was used to solve a similar problem. After analyzing this approach, we came to the conclusion that it does not provide sufficient adaptivity for our task when integrating functions with sharply varying integral expressions near singular regions. In this work, the Gauss–Kronrod method [6] was used, which, while maintaining the accuracy of the classical Gauss–Legendre scheme, additionally provides built-in error control and automatic refinement of integration nodes. This made it possible to increase the stability and accuracy of calculations of the Luneberg integral without the necessity of the sampling parameters manual adjustment, which is especially important for numerical optimization of profiles with arbitrary boundary conditions.

2.2.3. Lens Construction Examples

In this study, two cases were considered, namely when the source is at infinity and when the point source is located at a distance R_s from the center of the lens.

The flat front incident on the lens that is corresponds to the boundary condition $R_{src} \to \infty$. The final image radius $R_{img} = R_f$ is set in the calculation in order to required focus be formed at a point located on the axis outside the lens. The refractive index profile $n(R)$, found according to the numerical integration scheme, ensures the transformation of a parallel rays into a converging spherical wave. In this case, the trajectory of all rays is subject to the condition of conservation of optical moment, and the total refraction in a radially symmetric field creates equal focusing at a distance of R_f from the center.

In this case, the final radius of the source $R_{src} = R_s$ is set in the calculation, that is, the wave front is formed by a point source located outside the lens. The target condition requires the focus having radius $R_{img} = R_f$ be located outside the structure. In this case, the $n(R)$ profile transforms the initial spherical wave radiating from the source into a wave converging at a selected point behind the lens. Thus, the lens performs the function of double focusing, that is, it changes the trajectories in such a way that the optical length of all possible paths between the source at a distance of R_s and the focus at a distance of R_f remains the same.

If the radius of a circular lens R_0 is equal to *1.0*, then in order to focus a plane wave to a point located at a distance of half the radius from the lens boundary ($R_2 = 1.5$), a centrally symmetric distribution of conductivity inside this lens was constructed. It is shown in Figure 2 using the color correspondence scale that is placed in the right part of a figure.

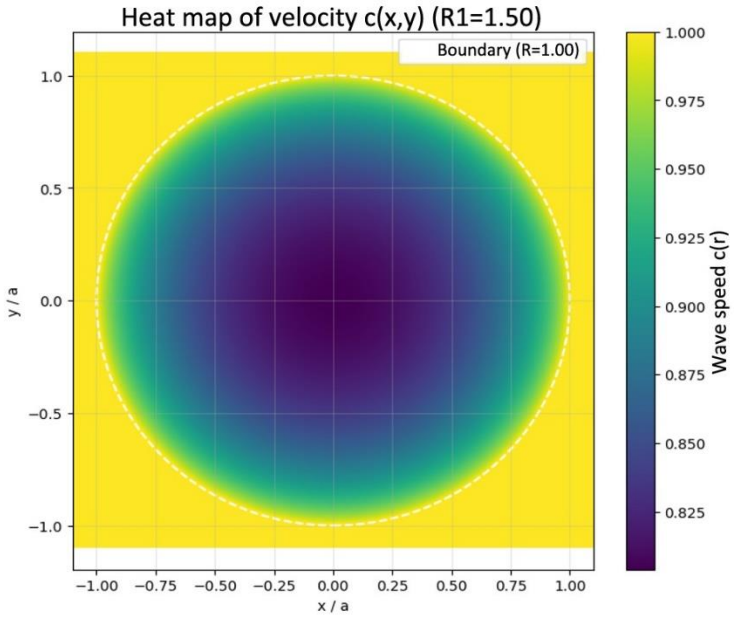

Figure 2.
The distribution of conductivity in a Luneberg lens focusing a plane wave to a point at a distance of 1.5 radii behind the lens. The correspondence of the color and conductivity of the medium is shown in the right part of the figure

The conductivity (velocity of propagation of disturbances) in the center of the lens was approximately *0.81*. For numerical simulation of the kinematics of the front of a two-dimensional wave passing through this cylindrical lens with such a distribution of conductivity, a method based on the Huygens principle was used [8, 9]. The essence of the numerical method is based on the fact that the nodes of the computational grid, where the wave-front has already reached, themselves

become wave sources, from which the disturbance radiates in all directions. The calculation was carried out in a *1000x600* node grid area with a spatial step of *0.005* m in both directions. The center of the lens with a radius of *1* m was located at the node *(300,300)*. The results of calculating the kinematics of an initially rectilinear wavefront, which coincides with the left boundary at the initial moment, are shown in Figure 3. If we assume that the speed of the wave outside the lens is *1* m/sec, then the wave travel times on the color vs conductivity scale (in the left side of the figure) is indicated in seconds.

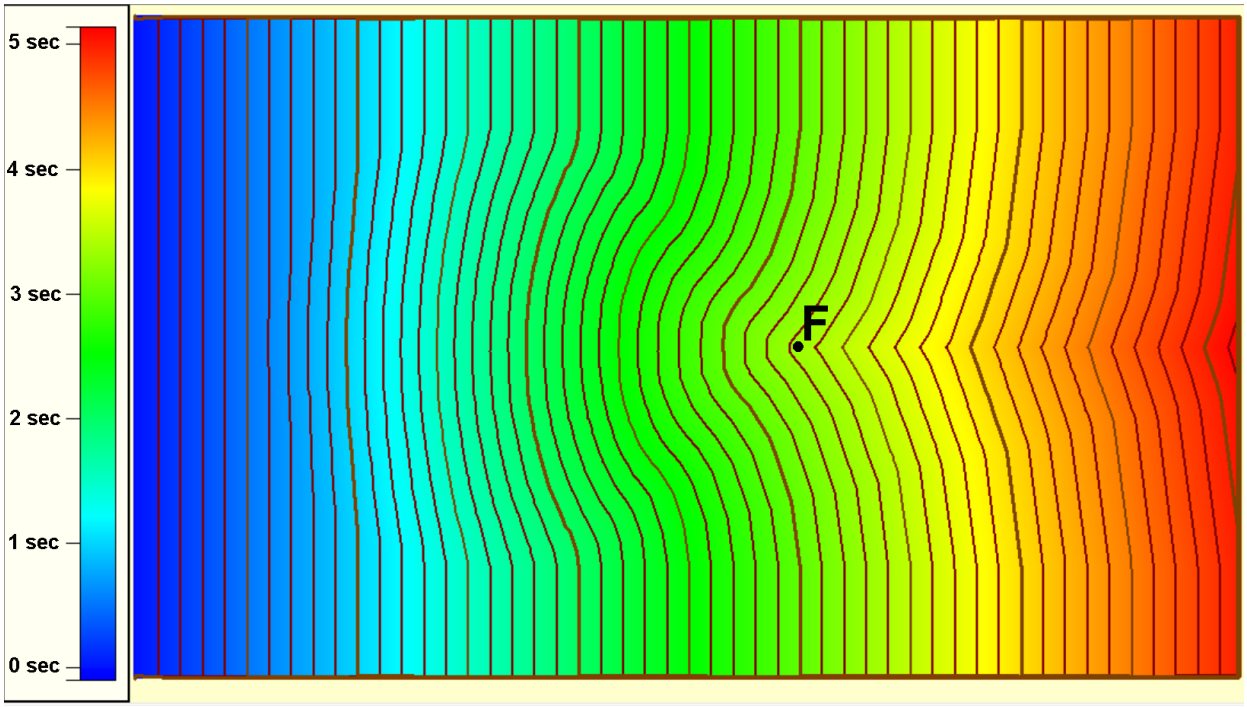

Figure 3.
Successive positions (in time) of the initially rectilinear wavefront as it passes through the Luneberg lens

Figure 3 shows that as the wave front passes over the lens, it curves, and a segment of the front with a width equal to the diameter of the lens converges to a single point (marked with the letter **F** in the figure).

2.3. Construction of Wave Rays That Pass a Luneberg Lens

To show that the mentioned segment of the wave-front is focused at a single point, we construct the wave rays using the step-by-step method of advancing the wave-front segment in orthogonal to the segment direction.

As is shown in Romanov [10] to find the trajectory of a ray in a two-dimensional inhomogeneous space exiting from a point (x_0,y_0), it is sufficient to solve a system of ordinary differential equations

$$\frac{dx}{dt} = \frac{\vec{p}_x}{n^2(x,y)}, \frac{dy}{dt} = \frac{\vec{p}_y}{n^2(x,y)}, \frac{d\vec{p}}{dt} = \nabla \ln n\,(x,y), \tag{9}$$

with initial conditions

$$(x,y)|_{t=0} = (x_0,y_0),\ \vec{p}|_{t=0} = n(x_0,y_0)\cdot\vec{v}^0, \tag{10}$$

where $\vec{v}^0$ – an arbitrary unit vector specifying the initial direction of the ray exit from the point (x_0,y_0). Here $\vec{p}$ – the normal vector to the wave-front, coinciding with the wave ray direction, $n(x,y) = 1/c(x,y)$ – refractive index, the inverse of the velocity of propagation of disturbances in the medium.

Let us propose another method for constructing wave rays in the case of an arbitrary distribution of conductivity. Let it be known at all points of the calculated ocean area. Accordingly, the propagation velocity of the wave front $c(x,y)$ is known. Consider a linear segment of length Δl, connecting the points A_0 and B_0 of the initial wave front (Figure 4). Set the calculated time step Δt. The next position of the edges A_1 and B_1 of the moving segment (wavefront segment) is determined as follows: the point A_0 moving to the distance $c(A_0)\cdot\Delta t$, while B_0 – to the distance $c(B_0)\cdot\Delta t$ in the direction of the external normal to the initial segment of the wave front. We connect the obtained points and at a distance $\Delta l/2$ from the middle of the obtained segment (point S_1) the points A_1 and B_1 are placed. After that, we repeat the construction and find the next position of the segment (A_2,B_2), having a point S_2 as its middle. Polyline S_0, S_1, S_2... can be considered as an approximate trajectory of the wave ray (Figure 4). We show that the polyline constructed in this way actually approximates the wave ray. Let us write out the change in the components of the ray direction vector $\vec{P}$:

$$\left(\frac{d\vec{P}}{dt}\right)_x = \vec{l}_x \frac{d}{dx} ln \frac{1}{c(x,y)} = -\vec{l}_x \frac{1}{c(x,y)} \cdot \frac{dc(x,y)}{dx}, \tag{11}$$

here $\vec{l}_x$ – the unit vector along the OX axis. It should also be taken into account that

$|\vec{P}| = \frac{1}{c(x,y)}$.

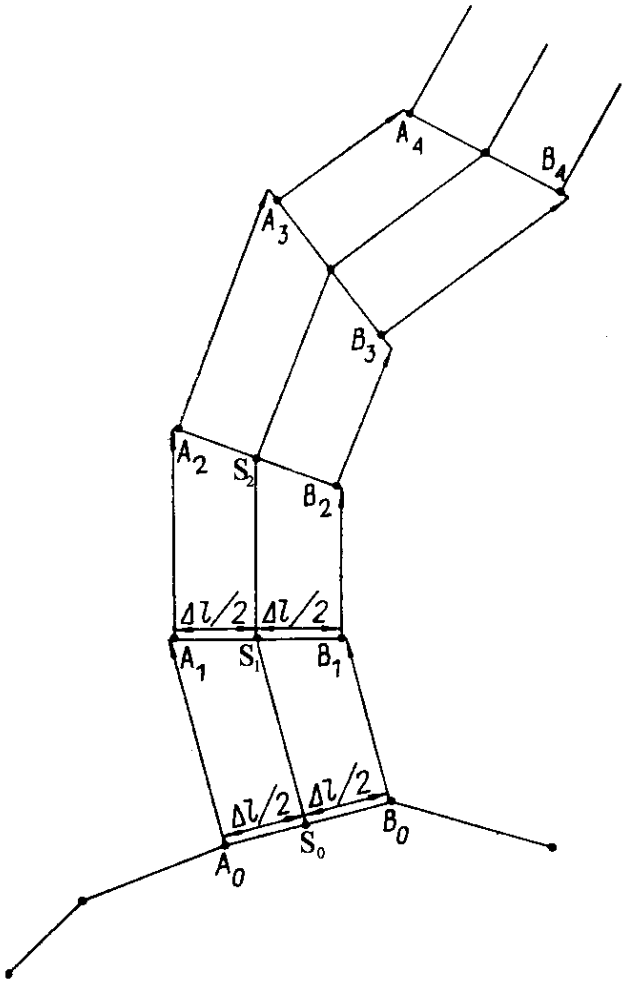

Figure 4.
Construction of a wave ray by moving a straight line segment.

Let be the next position at time t of the moving segment AB parallel to the OX axis (Figure 5). The length of the segment is Δl. According to the suggested method, during dt the point A moves to the distance $dt \cdot c(x,y)$, and the point B – to the distance $dt \cdot c(x+\Delta x,y)$, where (x, y) – the point A coordinates. The orthogonally directed to the segments AB and DE vectors $\vec{P}$ give the direction of the wave ray segments having lengthes 1/c. Let us construct both vectors $\vec{P}(x, y)$ and $\vec{P}(x, y + c(x, y)dt)$, outgoing from the point D. In Figure 5 these will be the segments BF and DG. The length of the segment DF is equal to $1/c(x, y)$, and the length of DG is equal to $1/c(D)$. The coordinates of point D are x and $y + c(x,y) \cdot dt$ by construction.

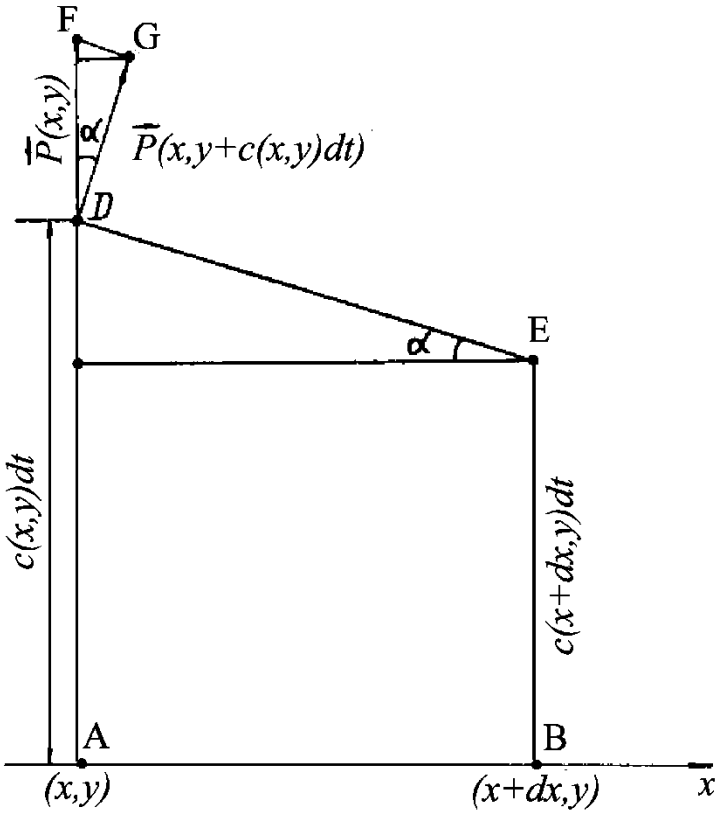

Figure 5.
Diagram of the movement of the wavefront segment in one time step.

Let us now find out how the projection on the OX axis of the segment FG, i.e. the vector $\vec{P}(t) - \vec{P}(t+dt)$ is expressed:

$$\left(\vec{P}(t+dt) - \vec{P}(t)\right)_x = \frac{1}{c(x,y+c(x,y)\cdot dt)} \cdot sin(\alpha) = -\frac{c(x,y)\cdot dt - c(x+\Delta x,y)\cdot dt}{c(x,y+c(x,y)\cdot dt)\cdot \Delta x}.$$

Thus,

$$\left(\frac{\vec{P}(t+dt)-\vec{P}(t)}{dt}\right)_x = -\frac{c(x+\Delta x,y)-c(x,y)}{\Delta x} \cdot \frac{1}{c(x,y+c(x,y)\cdot dt)}. \quad (12)$$

The lefthand side of Equation 12 approximates the component of the vector $\frac{d\vec{P}}{dt}$ along **OX** axis, and the first multiplier on the righthand side presents the derivative $\frac{dc}{dx}$. Thus, if we show that the second multiplier is also close in value to *1/c(x, y)*, this will mean that the wave ray direction changes in accordance with Equation 11 during the proposed construction. The first equation from (9) is fulfilled by virtue of the construction of the proposed method.

Let us return to the second multiplier of the right-hand side of Equation 12. It is necessary to evaluate the following difference:

$$\Delta S = \frac{1}{c(x,y+c(x,y)\cdot dt)} - \frac{1}{c(x,y)}. \quad (13)$$

Let us determine the order of magnitude of the derivative of the wave propagation velocity. In our problem, inside a lens with a radius of *1*, the conductivity of *c(x,y)* varies from *1* at the boundary to about *0.8* in the center. Therefore, we have the following an approximate estimate:

$$\left|\frac{\partial c}{\partial x}\right| \le 0.2, \qquad \left|\frac{\partial c}{\partial y}\right| \le 0.2 \quad (14)$$

If one choose the step *dt* such that the value *Δy = c(x,y)·dt* is small relatively to the length of the segment *Δx*, then the deviation of the second multiplier on the right side of equation (11) from *1/c(x, y)* is expressed as

$$\delta = \frac{c(x,y) - \left(c(x,y) + \frac{c(x,y+\Delta y)-c(x,y)}{\Delta y} c(x,y)\cdot dt\right)}{c(x,y)\cdot c(x,y+\Delta y)} \quad (15)$$

It follows from constraints (14) that the numerator in expression (15) does not exceed *0.2 c(x,y)·dt*. So, the relation (15) will be written as

$$\delta \leq \frac{0.2 \cdot dt}{c(x,y+\Delta y)} \qquad (16)$$

When using a sufficiently small time step *dt* in calculations supporting the wave advance no more than one step through space in one time step, the constructed ray will be quite close to the true one (solving the differential equation of the wave ray). In the calculation, the time step was equal to *0.003*. At the same time, for the smaller depth gradients the larger the time step can be used.

To plot the trajectories of rays passing through a Luneberg lens, consider a grid area of *1000 x 600* nodes, where the conductivity of the medium inside the lens is determined by the method described in the second section, and in the rest of the area it is equal to *1*.

The wave ray trajectories constructed by the described method for the case of focusing a flat wave to the focal point located behind the lens at a distance of *1.5* radii from the lens center are shown in Figure 6.

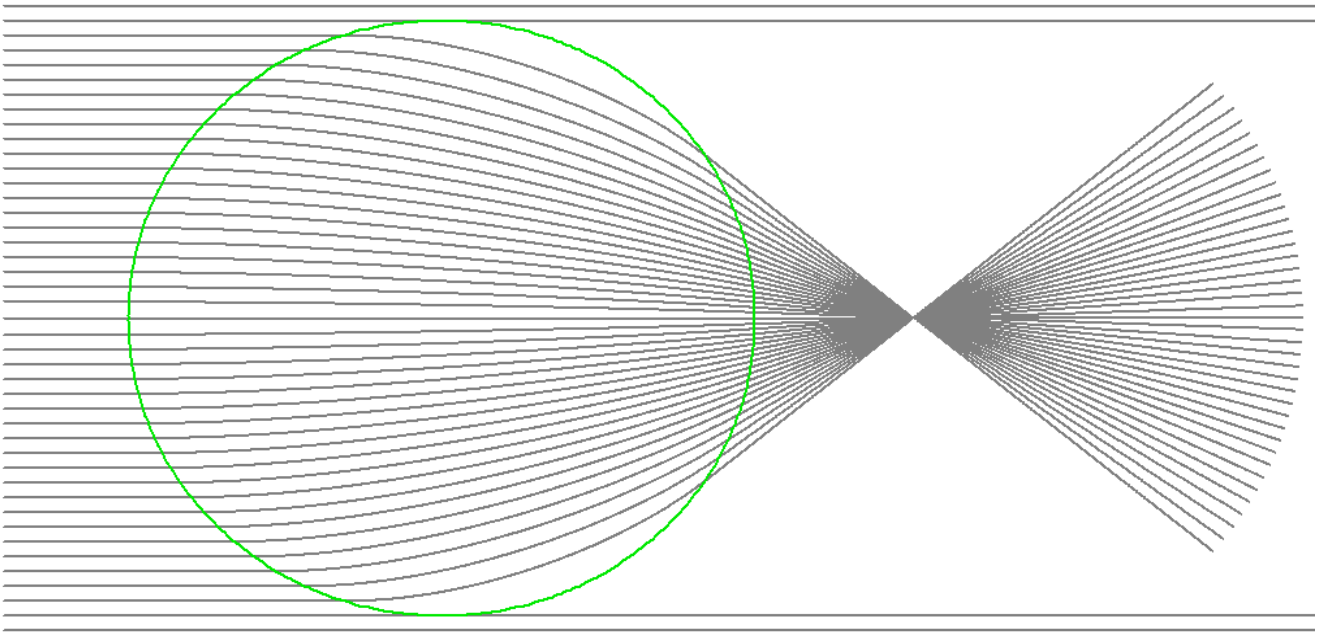

Figure 6.
Trajectories of wave rays of a plane wave coming from the left boundary of the region through a round Luneberg lens with optical conductivity, shown in Figure 2. The boundary of the lens is depicted as a green circle.

Consider another lens with radius $R_0 = 1$ that focuses a plane wave to a point at a distance of one lens diameter from its center. In this case, $R_1 = \infty$, and $R_2 = 2 \cdot R_0 = 2$. For these parameters, the distribution of conductivity inside the lens from the distance to its center is also constructed using the method described in section 2. After that, numerical simulation of the kinematics of the wave front and the construction of wave rays were carried out, the results of which are shown in Figure 7.

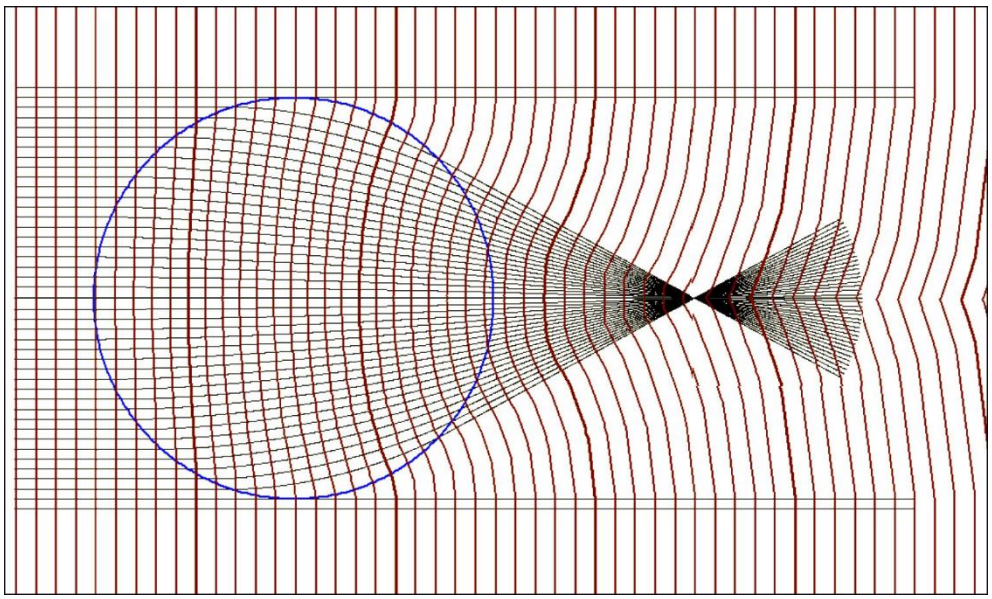

Figure 7.
A map of wave rays and fronts when focusing an initially flat wave with a Luneberg lens to a point located at a distance of its diameter from the center of the lens.

As can be observed from Figure 7, the constructed distribution of the medium conductivity inside the lens causes the initially flat wave to focus to a single point located at a distance of one radius behind the lens. This fully confirms the effectiveness of the Luneberg lens construction algorithm for focusing a plane wave at a given distance behind it.

3. Results

As was already mentioned, long waves in the ocean [11] (in particular, tsunamis), like electromagnetic waves, can be focused at one point under the influence of refraction, when the wave passes over an underwater mountain. Due to the fact that the propagation velocity of the long wave front does not depend on its amplitude and is determined by the formula [11]:

$$c(x,y) = \sqrt{gD(x,y)}, \tag{16}$$

where D is the depth and g is the acceleration of gravity, it is easy to construct a depth distribution over a circular seamount based on the velocity distribution found inside the Luneberg lens.

To do this, it is only necessary to express from Equation 5 the values of the depth $D(x,y)$ in terms of the values of the conductivity of the medium $c(x,y)$. Thus, we obtain an array of depth values for numerical simulation of the focusing of a long wave after its passage over this circular seamount. Wave propagation was modeled in the framework of a nonlinear shallow water model using the McCormack difference scheme [12, 13] in a gridded area of *1000x600* computational nodes. The grid step in both directions was *1000* m. The radius of the circular seamount centered at the node *(301,301)* was *200* spatial steps. In the computational experiment, a plane wave with a height of *0.5* m with a period of *300* seconds moved from the left border of the region and passed over this circular bottom elevation and, due to refraction, focused into the vicinity of a point located at a distance of *300* spatial steps from the center of the bottom irregularity. The position of the focus point obtained as a result of this computational experiment completely coincides with the theoretical estimate for the constructed lens. The results of the numerical calculation are shown in Figure 8 in the form of a distribution of wave height maxima over the entire computational domain.

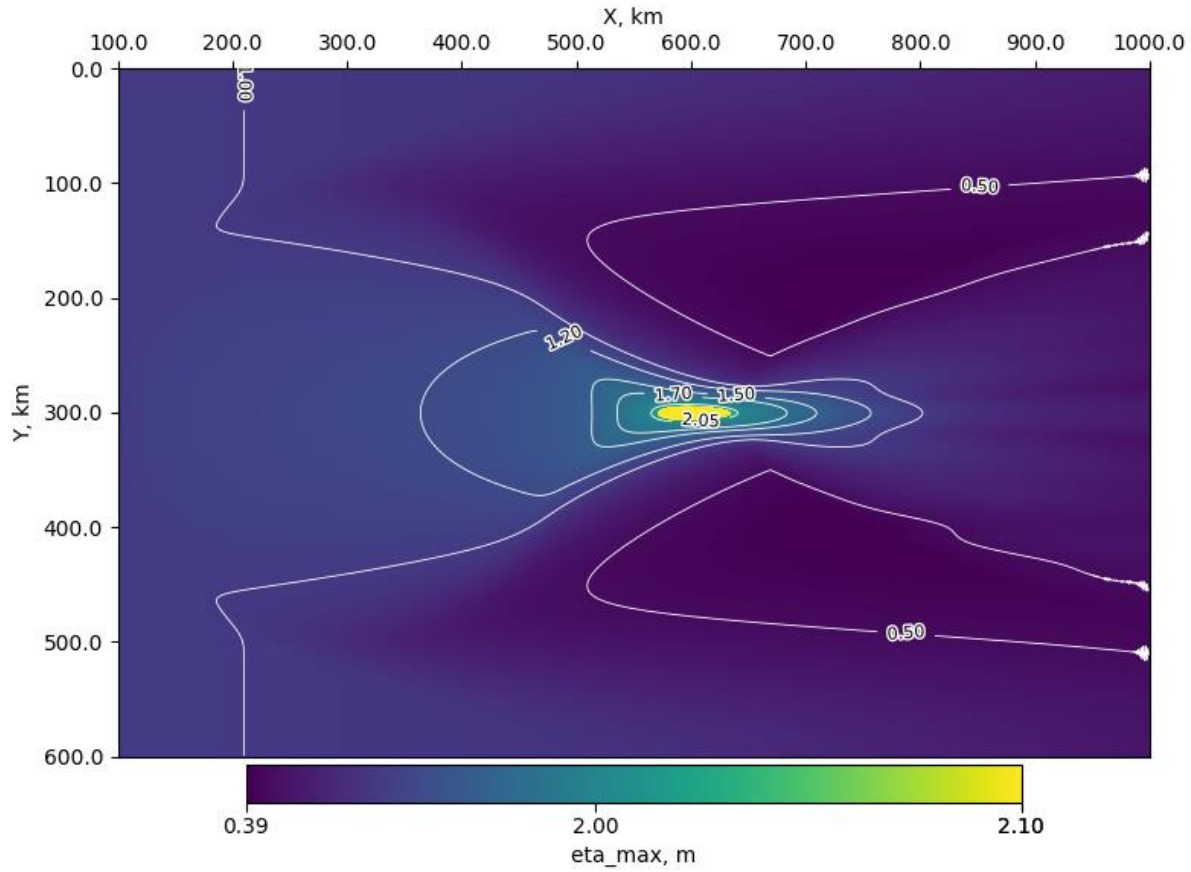

Figure 8.
Isolines of the distribution of the wave height maxima as a result of numerical simulation of the passage of the half-meter plane wave over a seamount acting on the wave as a Luneberg lens.

Let us consider another variant of the lens parameters, which leads to focusing a wave from a point (round-shaped) source located at a distance of $R_1 = 2R_0$ from the center of the lens to a point located at a distance of $R_2 = 3R_0$ on the opposite side of the lens. A circular lens with a radius of *200* spatial grid steps centered at *(1000,300)* is placed in a grid area measuring *1800* x *600* computational nodes. The distribution of conductivity inside the lens is calculated using formulas (5) – (6). In this case, the calculation of wave rays was carried out by numerically solving the differential equations of the wave ray using the Euler method [14]. Let us describe the method used in this case.

To discretize the system of equations of rays dynamics, a fixed time step Δt is introduced. This step sets discrete time points at which the coordinates and momentum of each ray are sequentially updated. The calculation process at each step can be described by a sequence of logical steps, which, however, are not strictly separated, but represent a single continuous numerical integration procedure.

At the first stage, the gradient of the refractive index n at the current point of the trajectory $(x^{(m)}, y^{(m)})$. is calculated. This gradient determines the direction of the change in the refractive field and, consequently, the direction of the change in the beam momentum. In the numerical implementation, the gradient $\nabla \ln n$ can be calculated in advance on the entire grid using the central difference method or estimated by interpolation during the transition between nodes. This step is expressed as a continuous numerical integration procedure

$$(\nabla \ln n)^{(m)} = \left(\frac{\partial}{\partial x}\ln n,\ \frac{\partial}{\partial y}\ln n\right)\Big|_{(x,y)=(x^{(m)},y^{(m)})}.$$

The obtained gradient value is used to update the momentum vector, which corresponds to an explicit Euler step. Here the current momentum is corrected to account for the local variation of the medium

$$\tilde{\vec{p}}^{\,(m+1)} = \vec{p}^{\,(m)} + (\nabla \ln n)^{(m)}\,\Delta t.$$

Next, a normalization procedure is applied to enforce the constraint $\| \vec{p} \| = n$. The predicted momentum $\tilde{\vec{p}}^{\,(m+1)}$ is rescaled to the local refractive index evaluated at the updated position:

$$\vec{p}^{\,(m+1)} = n(x^{(m+1)}, y^{(m+1)})\ \frac{\tilde{\vec{p}}^{\,(m+1)}}{\| \tilde{\vec{p}}^{\,(m+1)} \|},$$

The following stage consists in updating the ray coordinates. Using the known momentum and refractive index, the new trajectory point is found as

$$(x^{(m+1)}, y^{(m+1)}) = (x^{(m)}, y^{(m)}) + \frac{\vec{p}^{\,(m+1)}}{n^2(x^{(m)}, y^{(m)})}\,\Delta t.$$

The integration loop continues as long as the ray remains inside the computational domain. The march is terminated if the current point exits the bounds of the velocity matrix or the maximum number of steps is reached. In this way, a discrete trajectory is formed for each of the N rays.

In the computational experiments performed, the gradient $\nabla \ln n$ was precomputed over the entire grid, which significantly accelerated the tracing. Interpolation of n and ∇n ensured smooth trajectories in inter-node regions. The time step Δt was selected experimentally, based on the stability condition of the Euler method and the need to accurately reproduce the trajectory.

A similar approach has previously been used in ray problems where the Euler method was also applied [14]. In particular, the scheme described here can be regarded as a simplified realization of the four-component Pukhalskii method [15] in which the explicit Euler step is supplemented by a momentum normalization procedure that ensures the preservation of the energy invariant when numerically solving the equations of geometrical optics. This combination improves the stability and accuracy of computations when modeling ray propagation in smoothly inhomogeneous media.

As the baseline integrator for the ray equations, we chose the simple explicit Euler method. Its key advantage is algorithmic transparency: at each step we evaluate the gradient once, then update the vector $\vec{p}$ and the coordinates (x, y) via

$$\tilde{\vec{p}} = \vec{p} + \nabla \ln n\,\Delta t, \qquad (x, y) = (x, y) + \frac{\tilde{\vec{p}}}{n^2(x, y)}\,\Delta t,$$

and immediately normalize $\tilde{\vec{p}}$, enforcing $\| \vec{p} \| = n$.

Thanks to its simplicity, the Euler method has low computational cost: when tracing hundreds of rays with a step on the order of $0.5 \ldots 1$ grid spacing, the scheme responds instantly. For small Δt, the accumulated first-order error remains negligible. Although in terms of theoretical accuracy Euler is inferior to, e.g., Runge–Kutta schemes, it fully meets our needs: trajectories in a smooth field $n(x, y)$ are reproduced with an error below the visual threshold. Moreover, the algorithmic structure is modular, so Euler can be replaced by a higher-order scheme without changing the overall architecture of the tracer if needed.

Figure 9 shows computed wave-ray trajectories emitted by a point source located at $(400{,}300)$.

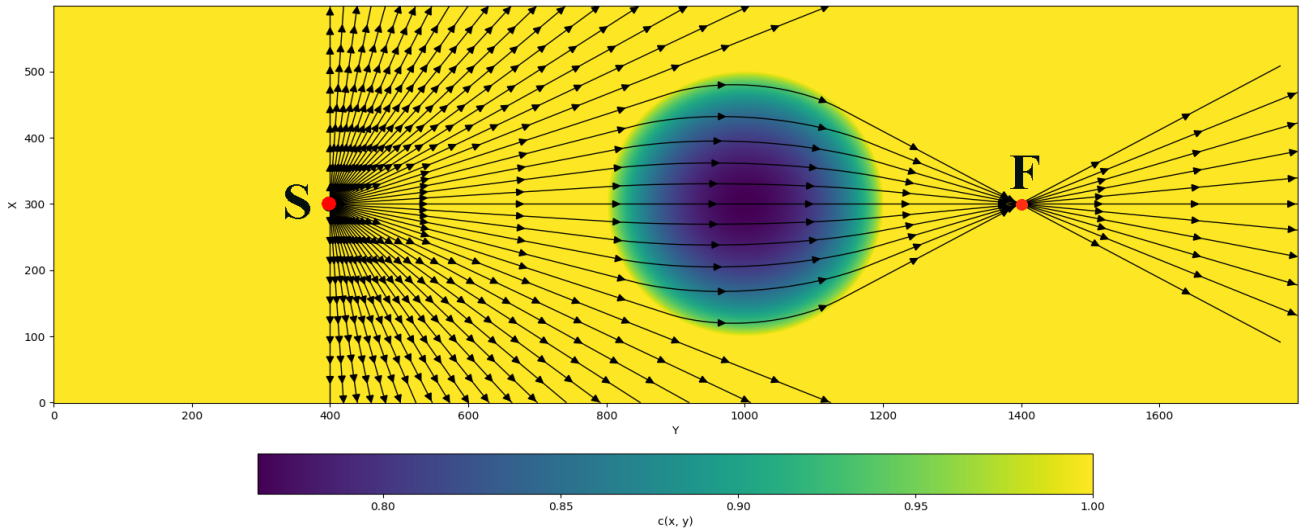

Figure 9. Visualization of wave rays from a point source located at a distance of three radii from the lens center. Arrow markers along the rays indicate wavefront positions at equal time instants. The color bar on the right shows the correspondence between color and the medium conductivity inside the lens.

The focusing properties of the constructed Luneburg lens were verified by simulating the propagation of a long wave from a circular source in a region with a submerged seamount that, according to formula (5), creates a conductivity field corresponding to a Luneburg lens. In a grid domain of size 1800×600 nodes with spatial steps $\Delta x = \Delta y = 1000$ m, we prescribe a circular seamount of radius 200 grid steps, centered at node $(1000{,}300)$. A long-wave source of radius 50 grid steps with the initial free-surface displacement at the center equal to 2 m is placed at $(400{,}300)$. The source generates a wave with a circular front, one sector of which is captured by the lens and, due to refraction, is then focused into the vicinity of the focal point located at a distance of three lens radii from its center. The distribution of maximum wave heights over the entire computational domain is shown in Figure 10.

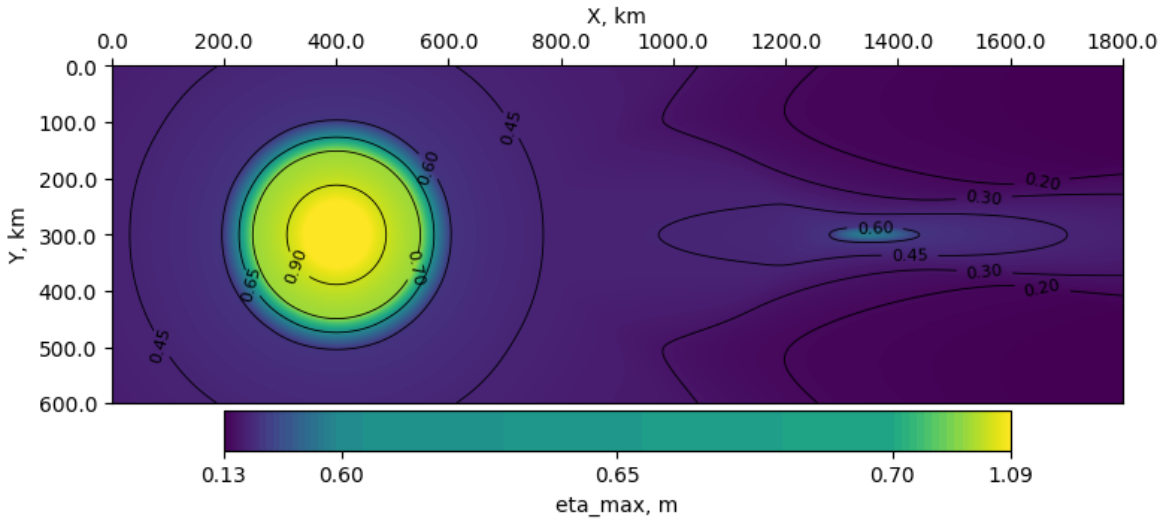

Figure 10.
Distribution of peak heights obtained in the numerical simulation of focusing a long wave from a circular source with its center at a distance $2r_0$ from the lens center into the vicinity of the point at a distance $3r_0$ from the same center on the opposite side of the lens. The color scale at the bottom shows the correspondence to wave heights.

As seen in Figure 10, in the vicinity of the point located at a distance $3R_0$ from the lens center, significantly higher waves are observed compared to other nodes of the computational region to the right of the lens. The distance between the lens center and the focal point fully agrees with the value specified when constructing the lens in Section 2, namely three lens radii.

4. Discussion

The construction of a Luneburg lens is a relevant task in the design of antennas for amplifying electromagnetic waves. In practice, implementing the required continuous variation of the refractive index within the lens is almost impossible. However, it is possible to design the lens layer by layer to achieve the desired properties.

The article described and tested a method that allows calculating the field of conductivity inside a Luneburg lens, which focuses a wave from a source located at a distance R_1 from the lens center into a point at a distance R_2 on the opposite side of the lens. In particular, if R_1 or R_2 is infinite, a spherical wave can be transformed into a plane wave, or vice versa.

Since only a portion of the radiation from the source that reaches the lens surface is focused, the intensity of the radiation at the focal point strongly depends on the distance from the point source to the lens.

The focusing properties of the lenses constructed in this work were verified by calculating the kinematics of wave rays and fronts, as well as through numerical modeling of long waves, where an underwater seamount acts as a lens that transforms a plane wave into a spherically converging one, subsequently focusing it near a single point. The calculations showed that in the case of focusing a plane long wave at a point located one and a half radii behind the lens, the wave height at that point was observed to be five times greater than the height of the original wave (see Fig. 8).

5. Conclusions

Constructing a Luneburg lens with prescribed properties is a nontrivial task for which no general closed-form formulas exist. We developed a numerical method to determine the distribution of conductivity (refractive index) inside the lens and verified its correctness by numerical simulations of wavefront and ray kinematics. Using the analogy between optics and the propagation of long surface gravity waves, we found the bathymetry of submerged seabed features that focus a wave with an initially rectilinear front into a single point (a neighborhood of a point), and we estimated the associated amplification of wave intensity. This should be taken into account by tsunami-warning services to avoid additional damage and loss of life.

References

[1] Y. A. Kravtsov and Y. I. Orlov, *Geometrical optics of inhomogeneous media*. Moscow: Nauka, 1980.
[2] S. V. Kuzmin, "Parameters of layers for a multilayer Luneburg lens," *Letters to Journal of Technical Physics,* vol. 30, no. 22, pp. 37–43, 2004.
[3] I. V. Grigoriev and I. V. Munina, "Cylindrical luneburg lens using additive technologies," *Electronics and Microwave Microelectronics,* vol. 1, pp. 606–611, 2021.
[4] E. G. Zelkin and E. A. Petrova, *Lens antennas*. Moscow: Sovetskoe Radio, 1974.
[5] N. H. Abel, "Note on a general integral transformation," *Journal Für Die Reine Und Angewandte Mathematik,* vol. 1, pp. 153–157, 1826.
[6] R. Piessens, E. de Doncker-Kapenga, C. W. Überhuber, and D. Kahaner, *QUADPACK: A subroutine package for automatic integration*. Berlin: Springer, 1983.

[7] G. Beliakov, "Numerical evaluation of the Luneburg integral and ray tracing," *Applied Optics*, vol. 35, no. 7, pp. 1011-1014, 1996. https://doi.org/10.1364/AO.35.001011
[8] G. Dantzig, "On the shortest route through a network," *Management Science*, vol. 6, no. 2, pp. 187–190, 1960.
[9] A. G. Marchuk, "Minimizing computational errors of tsunami wave-ray and travel time," *Science of Tsunami Hazards*, vol. 27, no. 4, pp. 12-24, 2008.
[10] V. G. Romanov, *Inverse problems for differential equations*. Novosibirsk: NSU, 1983.
[11] J. J. Stoker, *Water waves*. Moscow: Inostrannaya literatura, 1957.
[12] R. W. MacCormack and A. J. Paullay, "Computational efficiency achieved by time splitting of finite-difference operators," *AIAA Paper*, vol. 72, no. 154, pp. 1–10, 1972.
[13] M. M. Lavrentiev, K. F. Lysakov, A. G. Marchuk, and K. K. Oblauhov, "FPGA fast simulation of tsunami wave propagation," *Russian Journal of Cybernetics*, vol. 2, no. 1, pp. 14–25, 2021. https://doi.org/10.51790/2712-9942-2021-2-1-2
[14] A. A. Amosov, Y. A. Dubinsky, and N. V. Kopchenova, *Computational methods for engineers*. Moscow: Vysshaya Shkola, 1994.
[15] J. Puchalski, "Numerical determination of ray tracing: A new method," *Applied Optics*, vol. 31, no. 31, pp. 6789-6799, 1992. https://doi.org/10.1364/AO.31.006789